Adjoint-Based Aeroelastic Design Optimization Using a Harmonic Balance Method

Anand, N.; Rubino, A.; Colonna, Piero; Pini, M.

DOI
10.1115/GT2020-16208

Publication date
2020

Document Version
Proof

Published in
ASME 2020 Turbo Expo

Proceedings of ASME Turbo Expo 2020
Turbomachinery Technical Conference and Exposition
GT2020
September 21-25, 2020, Virtual, Online

GT2020-16208

ADJOINT-BASED AEROELASTIC DESIGN OPTIMIZATION USING A HARMONIC BALANCE METHOD

Nitish Anand*, **Antonio Rubino, Piero Colonna, Matteo Pini**
Propulsion & Power,
Faculty of Aerospace Engineering,
Delft University of Technology,
The Netherlands.
Email: n.anand@tudelft.nl

ABSTRACT

Turbomachinery blades characterized by highly-loaded, slender profiles and operating under unsteady flow may suffer from aeroelastic shortcomings, like forced response and flutter. One of the ways to mitigate these aeroelastic effects is to re-design the blade profiles, so as to increase aero-damping and decrease aero-forcing. Design optimization based on high-fidelity aeroelastic analysis methods is a formidable task due to the inherent computational cost. This work presents an adjoint-based aeroelastic shape-optimization framework based on reduced order methods for flow analysis and forced response computation. The flow analysis is carried out through a multi-frequency fully-turbulent harmonic balance method, while the forced response is computed by means of the energy method. The capability of the design framework is demonstrated by optimizing two candidate cascades, namely, i) a transonic compressor cascade and, ii) a supersonic impulse turbine rotor operating with toluene as working fluid, initially designed by means of the method of waves. The outcomes of the optimization show significant improvements in terms of forced-response in both cases as a consequence of aero-damping enhancement.

NOMENCLATURE

Symbols

A	amplitude
$\mathcal{F}$	fixed point iteration operator
$\mathcal{G}$	grid movement operator
H	harmonic-balance operator
I	identity matrix
$\mathcal{J}$	objective function
J	Jacobian
K	stiffness matrix
k	number of frequency
$\mathcal{M}$	mesh operator
N	total number of instances
$\hat{n}$	normal
p	pressure
$\mathcal{R}$	residual operator
R	rotation matrix
$\mathcal{S}$	surface operator
S	surface
T	transformation matrix
t	time
U	conservative variables
$\mathcal{V}$	volume operator
v	velocity
W	work-per-cycle
X	mesh coordinates
x	modal amplitude

Greek symbols

α	design variable vector
Δ	change in quantity

θ	rotation degree
ϕ	flow angle
τ	time period
Ω	cell volume
ω	angular velocity

Subscripts

alt	alternating
avg	average
base	baseline
CAD	computer aided design
CFD	computational fluid dynamics
d	damping
FR	forced response
f	forcing
grid	mesh grid
i	index
in	inlet
n	time instance index
opti	optimum
out	outlet
pitch	pitching
surf	surface
t	time
tot	total conditions
vol	volume

Superscripts

$*$	converged solution
$+$	plus
q	physical time index
T	transpose

INTRODUCTION

Forced response and flutter are recurrent aero-elastic limiting factors for turbomachinery blades with slender profiles, high-aspect ratio, and markedly unsteady loading. Blades of this type are increasingly adopted in turbomachines of modern aero-engines [1], as a consequence of the effort to abate emissions by simultaneously increasing efficiency and reducing engine weight. Forced response phenomena are of particular concern in rotors of rocket engines and of supersonic turbines for organic Rankine cycle (ORC) power systems [2], due to the very high Mach numbers and associated strong shock waves, which may induce blade excitations deriving from stator-rotor interaction.

From a physical standpoint, both flutter and forced response occur when the blade structure absorbs energy from the fluid and reaches high vibration levels [1]. To mitigate this issue, one of the solutions is to re-design the blade by increasing the aero-damping, while maintaining aerodynamic performance. Usually, these design adjustments are performed downstream of the detailed fluid dynamic design, if potential structural issues are identified through comprehensive transient aero-mechanical calculations. This process is computationally expensive and predominantly based on designers' experience and, as such, it can arguably lead to final blade designs that are sub-optimal with respect to both aerodynamic and aeroelastic performance. Efficient automated design optimization procedures which can concurrently deal with the fluid-dynamic and the structural design problem can therefore aid the development of new blade concepts.

Adjoint-based design methods are suited for this purpose, due to the possibility to perform gradient-based optimization efficiently. However, the cost of performing a single time-accurate aero-elastic computation is still excessive, making adjoint optimization a very demanding task. In the attempt to circumvent this issue, reduced order models for aero-elastic turbomachinery computations have been proposed [3, 4, 5, 6, 7], the vast majority of them being based on the so-called *energy method* [8]. This method enables flutter and forced response analysis with engineering accuracy by means of unsteady fluid-dynamic simulations. The method is based on the principle of energy conservation: the energy added by the flow-unsteadiness is equal to that dissipated by the vibrating blade [4, 9]. It is an alternative to the *modal reduction method*. The *energy method* can be used as an efficient adjoint-based aero-elastic design optimization procedure, if the cost involved in performing unsteady flow computations can be greatly decreased. This can be accomplished with a time spectral or harmonic-balance method [10]. This approach has already been documented in the literature. Reference [5], for instance, documents the use of adjoint-based optimization to concurrently improve the aero-elastic and aero-dynamic performance of a transonic fan blade. Reference [6] presents the validation of sensitivities for an aero-elastic objective function calculated with the adjoint method and related to a 3D turbine test case.

The harmonic balance implementations currently documented in the literature are based on a single-frequency transformation for computational efficiency. As a result, flutter cannot be studied because it is inherently a multi-frequency flow problem [11]. Another limitation is the assumption of frozen viscosity, which implies that the turbulence sensitivities are not resolved during the adjoint computations.

This paper documents a cost-effective adjoint-based optimization method and its application to aero-elastic design problems. The method is based on a multi-frequency harmonic balance solver for fully-turbulent flows [12, 13]. The method is capable of treating flows of fluids in both ideal and non-ideal thermodynamic states [14] and is implemented in the open-source software SU2. In works which preceded the development documented here, the FFD-box method was adopted for blade parametrization [12,13], while a CAD-based surface method was

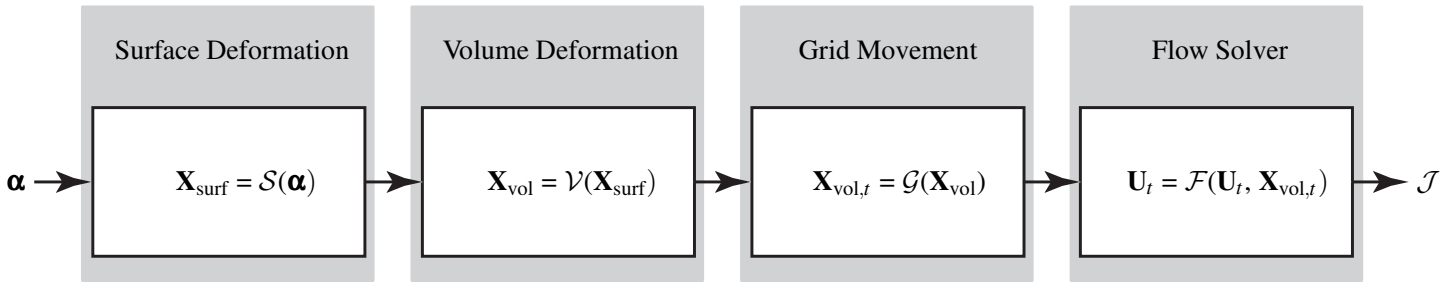

FIGURE 1: Simplified block scheme of the implementation of the fluid dynamic design chain (direct solver).

conceived and implemented subsequently and it has been employed in this research [15].

The capability of the method is demonstrated by performing forced response minimization of two exemplary test cases, i.e., i) a transonic compressor cascade, namely the tenth standard configuration taken from Ref. [16], and ii) a supersonic impulse turbine rotor operating with an organic working fluid, which is of interest because this type of turbine is employed in ORC power systems. The two test cases studied are characterized by slender blade profiles and strong shock-waves in the flow-domain, hence, are susceptible to aero-elastic effects.

METHOD

The methodology which was developed for this study can be described in three parts, namely, the part related to the direct solver, that related to the adjoint solver, and that related to the optimization. The algorithm implemented in the direct solver computes the solution of the flow equations and also morphs the mesh, in order to obtain the objective function. The adjoint solver provides the gradient of the objective function with respect to the design variables. The optimization algorithm utilizes the solutions and sensitivity values to obtain the result corresponding to the optimum design of the blade shape.

Direct Solver

The computational procedure implementing the design chain illustrated in Figure 1 uses the design variables vector $\boldsymbol{\alpha}$ as input and returns the objective function $\mathcal{J}$. It consists of four blocks, namely, surface deformation, volume deformation, grid movement and flow solver.

Surface Deformation. In order to deform the blade surface uniformly, a CAD-based parametrization method is used and the details of the method can be found in Ref. [15]. The parametrization algorithm is represented by the function $\mathcal{S}_{\text{CAD}}$ which operates on $\boldsymbol{\alpha}$, which is a vector made of blade design parameters like metal angles, chord and thickness distribution.

Using the surface parametrizer, the change in the surface grid ($\Delta\mathbf{X}_{\text{surf}}$) for the k^{th} design step is computed as

$$\Delta\mathbf{X}^k_{\text{surf}} = \mathcal{S}_{\text{CAD}}\left(\boldsymbol{\alpha}^k\right) - \mathcal{S}_{\text{CAD}}\left(\boldsymbol{\alpha}^{k-1}\right). \tag{1}$$

Subsequently, the surface coordinates ($\mathbf{X}_{\text{surf}}$) in the volumetric mesh for the k^{th} design step is given as

$$\mathbf{X}^k_{\text{surf}} = \mathcal{S}\left(\boldsymbol{\alpha}^k\right) = \mathbf{X}^{k-1}_{\text{surf}} + \Delta\mathbf{X}^k_{\text{surf}}. \tag{2}$$

Volume Deformation. A mesh-deformation algorithm manipulates the volumetric grid by means of a linear elasticity method implemented in SU2. The linear system of equations to be solved at optimization step k is given by

$$\mathbf{K}\Delta\mathbf{X}^k_{\text{vol}} = \mathbf{T}\Delta\mathbf{X}^k_{\text{surf}}, \tag{3}$$

where $\mathbf{K}$ is the stiffness matrix, $\mathbf{T}$ is the transformation matrix and $\Delta\mathbf{X}_{\text{vol}}$ is the change in the volume mesh. The vector $\Delta\mathbf{X}_{\text{surf}}$ is used as a Dirichelet boundary condition for the linear-elasticity solver. The mesh coordinates ($\mathbf{X}_{\text{vol}}$) corresponding to the k^{th} optimization step can be represented as

$$\mathbf{X}^k_{\text{vol}} = \mathcal{V}\left(\mathbf{X}^k_{\text{surf}}\right) = \mathbf{X}^{k-1}_{\text{vol}} + \Delta\mathbf{X}^k_{\text{vol}}. \tag{4}$$

Grid Movement. In order to simulate the unsteady motion of the blade due to vibrations, a deforming grid movement algorithm displaces the surface and the volume grid. The algorithm is the same as the one utilized for volume deformation. However, the change in surface mesh is provided by the grid movement procedure. More specifically, it is prescribed with a surface pitching subroutine in the simulations performed for this study. As a result, the linear system at time t for the k^{th} design step becomes

$$\mathbf{K}\Delta\mathbf{X}^k_{\mathrm{vol},t} = \mathbf{T}\Delta\mathbf{X}^k_{\mathrm{surf,pitch},t}, \tag{5}$$

and the volumetric mesh

$$\mathbf{X}^k_{\mathrm{vol},t} = \mathcal{G}\left(\mathbf{X}_{\mathrm{vol}}\right) = \mathbf{X}^k_{\mathrm{vol}} + \Delta\mathbf{X}^k_{\mathrm{vol},t}. \tag{6}$$

Flow Solver. The unsteady flow solution is computed by using a time-domain Harmonic Balance (HB) solver. The final form of the RANS equations, discretized using the HB method described in Ref. [12], can be written as

$$\left(\frac{\Omega I}{\Delta t} + \mathbf{J}\right)\Delta\mathbf{U}_n = -\tilde{\mathcal{R}}_n\left(\mathbf{U}^q, \mathbf{U}^{q-1}\right), \qquad n = 0, 1, ..., N-1, \tag{7}$$

in which Ω is the computational cell volume, Δt is the pseudo-time step [10], $\mathbf{J}$ is the flow Jacobian, q is the physical time index, N is the number of resolved time instances, and $\tilde{\mathcal{R}}$ is the residual operator defined as

$$\tilde{\mathcal{R}}_n\left(\mathbf{U}^q, \mathbf{U}^{q-1}\right) = \mathcal{R}_n\left(\mathbf{U}^q\right) + \Omega\sum_{\mathrm{i}=0}^{N-1} H_{n,i}\Delta\mathbf{U}_i + \Omega\sum_{\mathrm{i}=0}^{N-1} H_{n,i}\mathbf{U}^q_i. \tag{8}$$

In (8), H is the harmonic balance operator, calculated for a known set of k input frequencies corresponding to $N = 2k+1$ time instances. $\mathbf{U}$ is the vector of conservative variables and it includes both laminar and turbulent quantities and $\Delta\mathbf{U} = \mathbf{U}^q - \mathbf{U}^{q-1}$.

Equation (7) is reformulated in terms of a fixed-point iteration as

$$\mathbf{U}^{q+1}_n = \mathcal{F}_n\left(\mathbf{U}^q\right), \tag{9}$$

where $\mathcal{F}$ is a fixed point iteration operator. According to the Banach fixed-point theorem, Eqn. (9) admits a unique fixed-point solution $\mathbf{U}^*$ such that

$$\tilde{\mathcal{R}}_n\left(\mathbf{U}^*, \mathbf{U}^{*-1}\right) = 0 \iff \mathbf{U}^* = \mathcal{F}_n(\mathbf{U}^*, \mathbf{X}). \tag{10}$$

Adjoint Solver

The design chain whose implementation is illustrated in Figure 1 corresponds to the minimization problem

$$\min_{\alpha} \quad \mathcal{J}\left(\mathbf{U}_n(\boldsymbol{\alpha}), \mathbf{X}_{\mathrm{vol},n}(\boldsymbol{\alpha})\right), \tag{11}$$

$$\text{s.t.} \quad \mathbf{U}_n(\boldsymbol{\alpha}) = \mathcal{F}_n\left(\mathbf{U}(\boldsymbol{\alpha}), \mathbf{X}_{\mathrm{vol}}(\boldsymbol{\alpha})\right), \tag{12}$$

$$\mathbf{X}_{\mathrm{vol},n}(\boldsymbol{\alpha}) = \mathcal{M}_n(\boldsymbol{\alpha}) = \mathcal{G}\left(\mathcal{V}\left(\mathcal{S}(\boldsymbol{\alpha})\right)\right), \tag{13}$$

where, $\mathcal{M}$ is a differentiable function [13] which includes surface deformation, volume deformation and grid movement. The application of the Lagrange Multipliers method to derive the adjoint equations gives the flow and mesh adjoint equations in the form

$$\bar{\mathbf{U}}_n = \frac{\partial\mathcal{J}}{\partial\mathbf{U}_n}^{\mathrm{T}} + \sum_{\mathrm{i}=0}^{\mathrm{N}-1}\frac{\partial\mathcal{F}_i}{\partial\mathbf{U}_n}^{\mathrm{T}}\bar{\mathbf{U}}_i, \tag{14}$$

$$\bar{\mathbf{X}}_n = \frac{\partial\mathcal{J}}{\partial\mathbf{X}_n}^{\mathrm{T}} + \frac{\partial\mathcal{F}_n}{\partial\mathbf{X}_n}^{\mathrm{T}}\bar{\mathbf{U}}_n, \tag{15}$$

where $\bar{\mathbf{U}}_n$ and $\bar{\mathbf{X}}_n$ are the flow and mesh adjoint variables. After solving the adjoint equations, the sensitivity of the objective function with respect to the volume mesh can be written as

$$\frac{\mathrm{d}\mathcal{J}}{\mathrm{d}\boldsymbol{\alpha}} = \left[\frac{\mathrm{d}}{\mathrm{d}\boldsymbol{\alpha}}\mathcal{M}^{\mathrm{T}}_n(\boldsymbol{\alpha})\bar{\mathbf{X}}_n\right]. \tag{16}$$

Subsequently, the sensitivity of the volume mesh with respect to $\boldsymbol{\alpha}$ can be computed as

$$\frac{\mathrm{d}\mathcal{M}_n}{\mathrm{d}\boldsymbol{\alpha}} = \frac{\mathrm{d}\mathbf{X}_{\mathrm{vol},n}}{\mathrm{d}\mathbf{X}_{\mathrm{vol}}}\frac{\mathrm{d}\mathbf{X}_{\mathrm{vol}}}{\mathrm{d}\mathbf{X}_{\mathrm{surf}}}\frac{\mathrm{d}\mathbf{X}_{\mathrm{surf}}}{\mathrm{d}\boldsymbol{\alpha}}, \tag{17}$$

where, the term $\frac{\mathrm{d}\mathbf{X}_{\mathrm{vol},n}}{\mathrm{d}\mathbf{X}_{\mathrm{vol}}}$ and $\frac{\mathrm{d}\mathbf{X}_{\mathrm{vol}}}{\mathrm{d}\mathbf{X}_{\mathrm{surf}}}$ is obtained by means of algorithmic differentiation, and $\frac{\mathrm{d}\mathbf{X}_{\mathrm{surf}}}{\mathrm{d}\boldsymbol{\alpha}}$ is obtained with the complex-step method within the CAD-based surface parametrizer.

Optimization

The forced response amplitude is calculated with the energy method, which must be supplied with the value of work-per-cycle obtained with two unsteady simulations, namely, the one corresponding to aero-forcing and the one corresponding to aero-damping.

Test Case	ω [rads/sec]	A_f [-]	A_d [-]	ϕ_{in} [°]	$p_{tot,in}$ [Pa]	$T_{tot,in}$ [K]	p_{out} [Pa]
Transonic Compressor Cascade	6.28	0.01	2.0	45	30e5	580.0	0.8e5
Supersonic Impulse Turbine rotor	62.83	0.001	1.0	60	1e5	288.1	0.8e5

TABLE 1: Unsteady variables and boundary conditions for the two test cases.

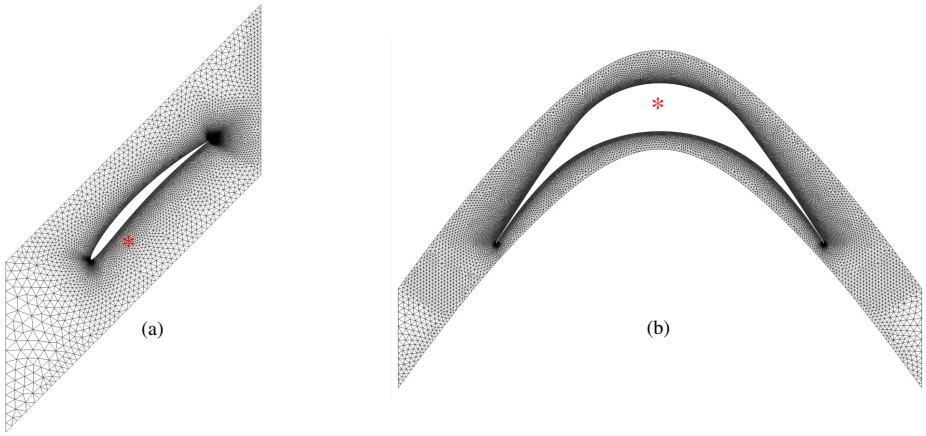

FIGURE 2: Discretized flow domain. The red asterisk indicates the intersection of the pitching axis with the flow domain, (a) transonic compressor cascade, (b) supersonic impulse turbine rotor.

The aerodynamic work is computed as

$$W = \int_t \oint_S -p \ \left(\hat{n} \cdot v_{\text{grid}}\right) \ \mathrm{d}S \ \mathrm{d}t, \tag{18}$$

where, p is pressure, $\hat{n}$ is normal and v_{grid} is grid velocity.

The unsteady aerodynamic forcing calculation is performed on a non-vibrating blade under the influence of unsteady pressure at the blades natural frequency (necessary condition for resonance), while the aerodynamic damping calculation is carried out on a blade vibrating at its natural frequency with a modal amplitude of x_{CFD} in a uniform flow. In this study, a realistic value of x_{CFD} is used to simulate the vibrating blade at an inter blade phase angle of 0.

The resulting solution from the two unsteady simulations are used to compute the work-per-cycle using equation (18). The work associated with aerodynamic forcing (W_f) is the energy transferred to the blade structure due to the flow unsteadiness, while the aerodynamic damping work (W_d) is the energy dissipated by the vibrating blade. The forced response (x_{FR}) of a vibrating blade is defined, according to the energy method, as

$$x_{\text{FR}} = \frac{W_f}{-W_d} \cdot x_{\text{CFD}} \tag{19}$$

where, x_{CFD} is the modal amplitude imposed on the CFD mesh during damping calculation [4].

The forced response minimization problem can be written as

$$\min_{\alpha} \ \mathcal{J}_{\text{FR}} = x_{\text{FR}}, \tag{20}$$

$$\text{s.t.} \ \ W_f > 0, \tag{21}$$

$$W_d < 0, \tag{22}$$

where, $\mathcal{J}_{\text{FR}}$ is the displacement amplitude computed with equation (19). The inequality constraints are imposed to prevent the inversion of signs during the optimization, which would change the physics of the problem.

The sensitivity of the objective function is computed by differentiating $\mathcal{J}_{\text{FR}}$ with respect to the design variables $\boldsymbol{\alpha}$ and its expanded form is

$$\frac{\mathrm{d}\mathcal{J}_{\text{FR}}}{\mathrm{d}\boldsymbol{\alpha}} = \left[\frac{\mathrm{d}\mathcal{J}_{\text{FR}}}{\mathrm{d}\mathbf{X}_{\text{surf}}}\right]_{\text{CFD}} \cdot \left[\frac{\mathrm{d}\mathbf{X}_{\text{surf}}}{\mathrm{d}\boldsymbol{\alpha}}\right]_{\text{CAD}}, \tag{23}$$

which symbolize (16). The sensitivity of the objective function with respect to the surface $\dfrac{\mathrm{d}\mathcal{J}_{\text{FR}}}{\mathrm{d}\mathbf{X}_{\text{surf}}}$ can be further expanded as

$$\left[\frac{\mathrm{d}\mathcal{J}_{\text{FR}}}{\mathrm{d}\mathbf{X}_{\text{surf}}}\right]_{\text{CFD}} = \left[-\frac{1}{W_d}\frac{\partial W_f}{\partial \mathbf{X}_{\text{surf}}} + \frac{W_f}{W_d^2}\frac{\partial W_d}{\partial \mathbf{X}_{\text{surf}}}\right] \cdot x_{\text{CFD}}. \tag{24}$$

The right-hand side of equation (24) can be calculated once the the direct and the adjoint solutions have been obtained.

CASE STUDIES

The described optimization framework is applied to two exemplary test cases: a *transonic compressor cascade*, commonly known as the tenth standard configuration of the AGARD Manual [16], and an *supersonic impulse turbine rotor* designed with the method of waves [17] and operating with toluene as the working fluid.

In the two cases, the aero-forcing calculation was performed by modulating the inlet total pressure according to the equation

$$p_{\text{tot,in},t} = p_{\text{tot,in}} \left[1 + A_{\text{f}} \sin(\omega t)\right], \tag{25}$$

where, A_{f} is the amplitude of the pressure perturbation, ω is the angular velocity corresponding to the natural frequency of the blade and t is the time instance. Additionally, the aero-damping calculation is performed by pitching the blade surface about the defined axis, therefore the surface coordinates and the pitch angle are

$$\mathbf{X}_{\text{surf},t} = \mathbf{X}_{\text{surf}}\, \mathbf{R}\left(\theta_{\text{pitch},t}\right), \tag{26}$$

$$\theta_{\text{pitch},t} = A_{\text{d}} \sin\left(\omega t\right). \tag{27}$$

where, $\mathbf{R}$ is the rotation matrix and A_{d} is the pitching amplitude. The pitching axis chosen for the two test cases is indicated with an asterisk in Figure 2.

To perform CFD calculations, the flow domain is discretized using quadrilateral elements close to the blade surface so as to maintain $y^+ < 1$ and triangular elements in the rest of the flow domain [18]. The discretized flow domain, consisting of 27,040 and 36,306 elements for transonic compressor and supersonic impulse turbine respectively, is shown in Figure 2. The flow was modeled with the Reynolds Averaged Navier-Stokes (RANS) equations and turbulence equations were closed using the Spalart-Allmaras model [19]. The unsteady flow term is solved using the HB method treated in Ref. [12].

The unsteady settings related to aero-forcing and -damping calculations, along with the boundary conditions, are tabulated in Table 1. A maximum of 10K iterations is set for both the simulations to assure a convergence of three orders of magnitude. For smooth convergence, mandatory for adjoint computations, the Euler semi-implicit time marching scheme with a CFL of 1.0 is used. The CFD simulations were performed with workstation equipped with an Intel Xeon Processor E5-2687W v3 (3.1 GHz, 20 cores).

RESULTS

The minimization problem defined by equation (20) was solved for the two test cases using the SLSQP optimization algorithm [20] available in the Python SciPy [21] library. In order to enable smooth convergence, both the objective and the constrain sensitivities were under-relaxed by a factor of 5e-3 and for simplicity only the thickness distribution is used as design variable.

Transonic Compressor Cascade

The work-per-cycle sensitivity of eight design variables, consisting of blade metal angles and thickness distribution, from the aero-forcing and aero-damping simulations were validated against gradients calculated with forward-finite-differences, using a step size of 0.001. Figure 4 illustrates the gradient validation for aero-forcing (•) and aero-damping (★). The adjoint-based sensitivities are plotted on the x-axis while the ones obtained using finite-differences on the y-axis. It can be observed that the value of the sensitivities are in good agreement, suggesting that the differentiation of the flow solver was performed correctly and that the adjoint-solver reached sufficient convergence. Reaching convergence with the direct solver required 93 minutes and 15 GB of RAM, while the adjoint solver required 366 minutes and 18 GB of RAM for one design step.

Figure 5 illustrates the optimization history of the forced response minimization. The value of the objective function $\mathcal{J}_{\text{FR}}$ (■) was reduced by 70% in 16 design steps, as a consequence of a reduction of the aero-forcing work (•) by more than 50% and of an increase of the aero-damping by a factor of ∼2.5 (▲).

The Mach number contours related to the flow around the baseline geometry and to aero-forcing and -damping simulations are illustrated in Figure 3. The flow accelerates from Mach 0.8, close to the leading edge, to a maximum of 1.1 on the suction side, triggering the formation of a shock in the front part of the blade. It can be seen that in the aero-forcing simulations the position and the strength of the shock varies in time (see Figure 3(a)). This is due to the change in the velocity magnitude at the inflow as a result of the fluctuating inlet total pressure.

Similar flow features can be observed in relation to the results of the aero-damping simulations (see Figure 3(b)). However, the change in the shock strength and position is due to the change in the angle of attack induced by the pitching motion.

Figure 6 illustrates the baseline geometry and the optimized geometry. The blade thickness increases along the blade in the optimized geometry and the majority of the shape changes are located close to the pitching axis, between chord-length 0.2 and 0.4.

Figure 7 shows the mean and the alternating surface pressure, for the two aerodynamic simulations using the baseline and the optimized geometry. In the figure, negative x-axis values represent the pressure side. The sudden change in pressure at

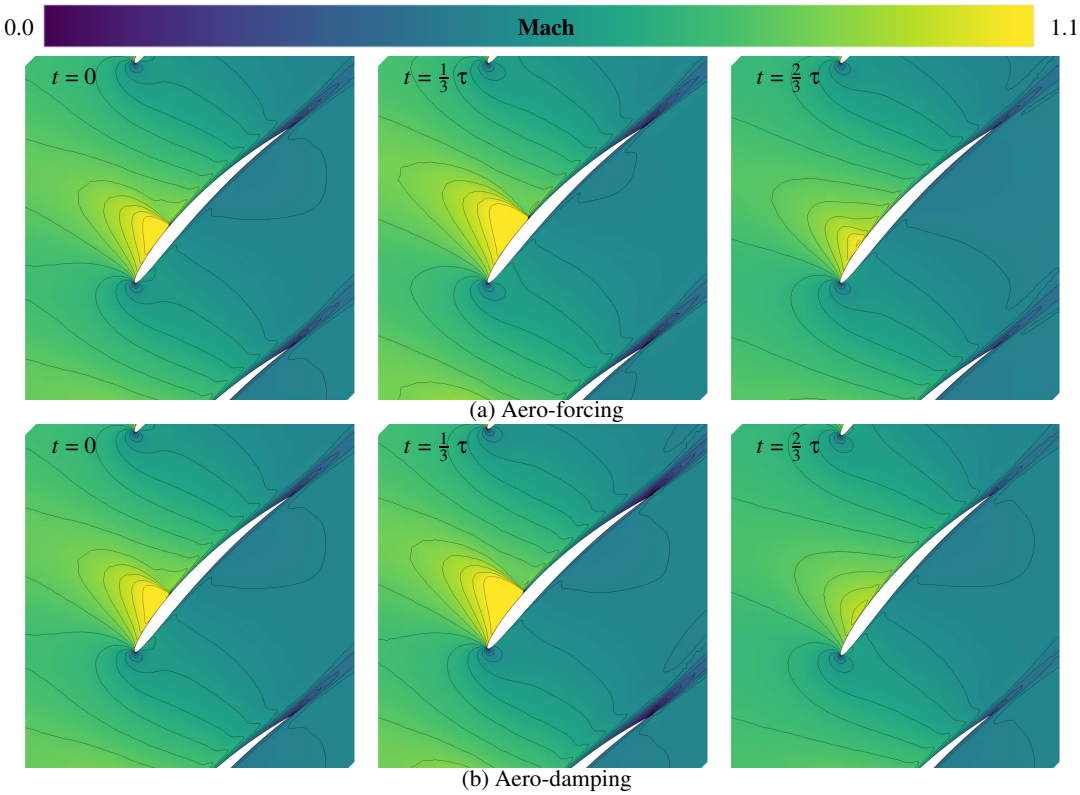

FIGURE 3: Mach number contours of the baseline geometry for transonic compressor cascade at three time slices, $t = 0$, $\tau/3$, $2\tau/3$ from left to right, (a) Aero-forcing, (b) Aero-damping.

chord length ∼0.25 is caused by the suction side shock-wave, as depicted in Figure 3. Due to the unsteadiness deriving from the pitching motion as well as from the total pressure variation, the shock-wave induces a relatively high value of the alternating pressure (Figure 7, bottom).

The highest variations of the mean and alternating pressure in the optimized geometry for the aero-forcing and -damping are confined between the leading edge and one-quarter of the chord (see Figure 7, dash-lines overlap). Additionally, it can be observed that the shock at chord-length ∼0.25 in the baseline geometry moves downstream in the optimized geometry. This is due to the increase of the blade thickness, see Figure 6, which leads to a smoother flow acceleration on the suction side. Furthermore, the optimization process causes an attenuation of simulated flow unsteadiness, which can be inferred from the reduction of the alternating pressure, as depicted in Figure 7.

Figure 8 shows the work distribution for the baseline and the optimized blade, as obtained with the aero-forcing and -damping computations. It can be seen that the shock-wave causes significant deviation of the work distribution in the front part of the blade. Moreover, the optimization leads to a flattening of the aero-forcing work (see Figure 8, top), while enhancing the negative values of the aero-damping work (see Figure 8, bottom). This is eventually beneficial for the aero-elastic behaviour of the blade.

Supersonic impulse turbine rotor

The validation of the adjoint-based gradients was not repeated for this test case because the results related to the compressor test case gave sufficient confidence about the accuracy of the method implementation. In this case the direct solver required 66 minutes and 14 GB RAM, while the adjoint solver required 216 minutes and 18 GB RAM for one design step.

The Mach number contours related to the flow around the blade obtained with the aero-forcing and -damping simulations for three time-instances are illustrated in Figure 10. The flow pattern indicates that the cascade is operating in the started flow regime [22], which is characterized by a shock-wave originating at the leading edge. The shock wave is then reflected multiple times along the flow passage. In the aero-forcing simulation, the variation of the total inlet pressure leads to a change in shock-wave strength, angle and Mach contour. The same can be observed in relation to the flow field computed with the aero-damping simulation in Figure 10, (b) as a result of the change in the incidence angle due to the pitching motion.

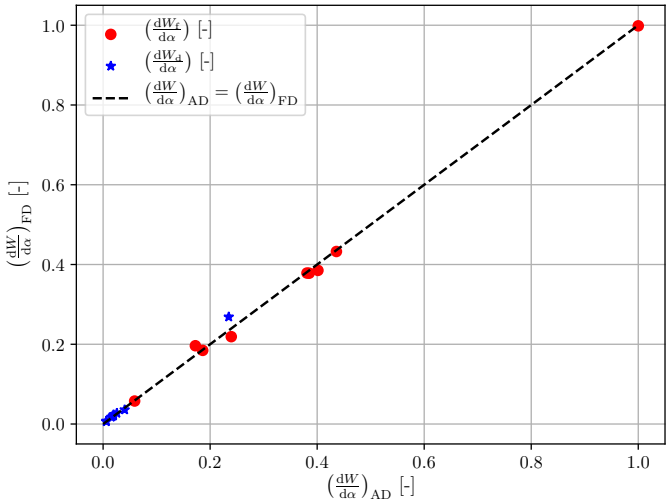

FIGURE 4: Validation of the work-per-cycle for the transonic compressor cascade; ★ indicates the damping work and ● indicates the forcing work.

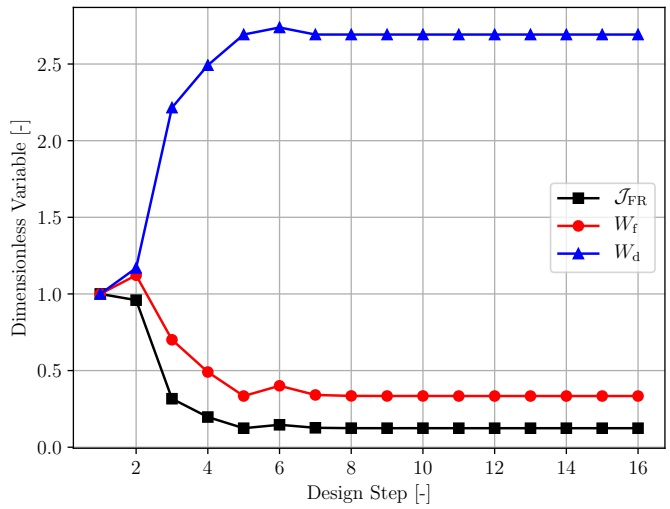

FIGURE 5: Optimization history of the forced response minimization related to the transonic compressor cascade.

Figure 9 shows the optimization history. Note that $\mathcal{J}_{FR}$ (■) is reduced by almost 60% in 10 design steps, as a consequence of an increase of W_d (▲) by 4 times, which counterbalances the increase of W_f (●) by 1.5 times.

The mean and the alternating surface pressure distribution related to the two unsteady simulations is illustrated in Figure 11. The x-axis represents the non-dimensional chord-length, with $x = 0$ being the position of the leading edge and the positive and negative values representing the suction and the pressure side, respectively. In the mean pressure plot (see Figure 11, top) the

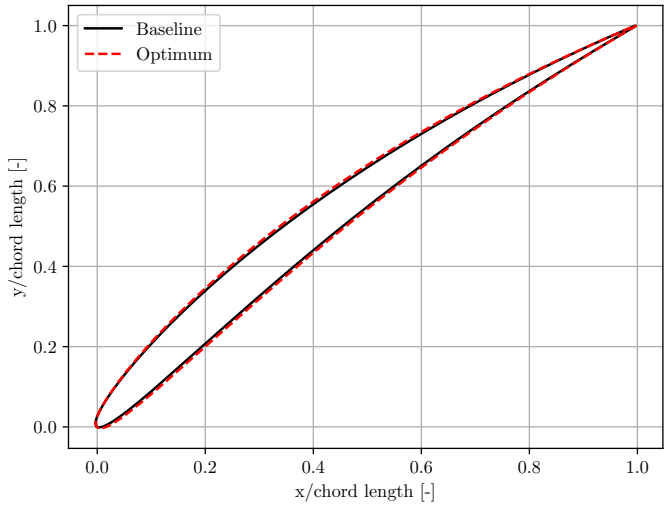

FIGURE 6: Baseline (solid) and optimum (dashed) blade geometry of transonic compressor cascade.

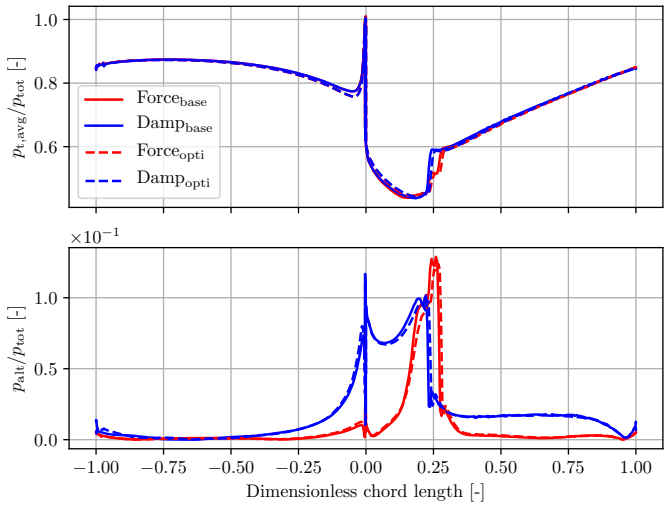

FIGURE 7: Time averaged (top) and alternating surface pressure (bottom) related to aero-forcing (red) and -damping (blue) simulations, for the baseline (solid) and the optimized (dashed) geometries. Negative and positive values of the chord length refer to the pressure and the suction side, respectively.

abrupt pressure changes are due to the shock reflection. The alternating pressure values are negligible close to leading edge (see Figure 11), primarily due to the absence of unsteady effects prior the first shock-wave impingement. In contrast, the rest of the flow field and the alternating pressure distribution in the rear part of the blade remarkably change. Moreover, the amplitude of the alternating pressure is much lower for forcing calculations if compared to that resulting from the damping calculations, due to

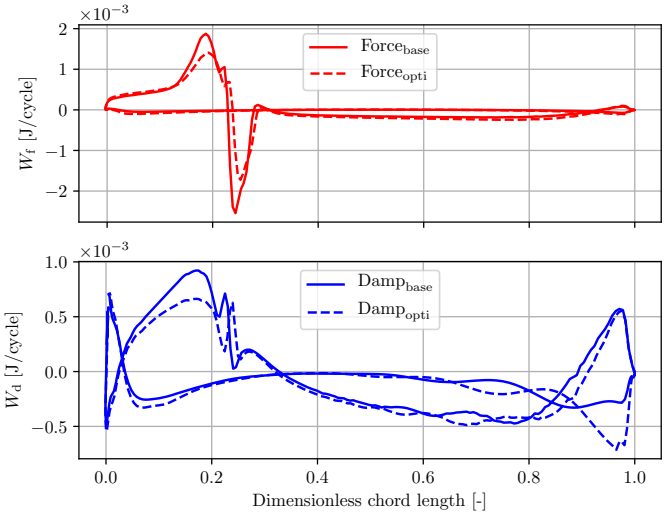

FIGURE 8: Local work for aero-forcing and -damping aerodynamic computations related to the transonic compressor cascade test case.

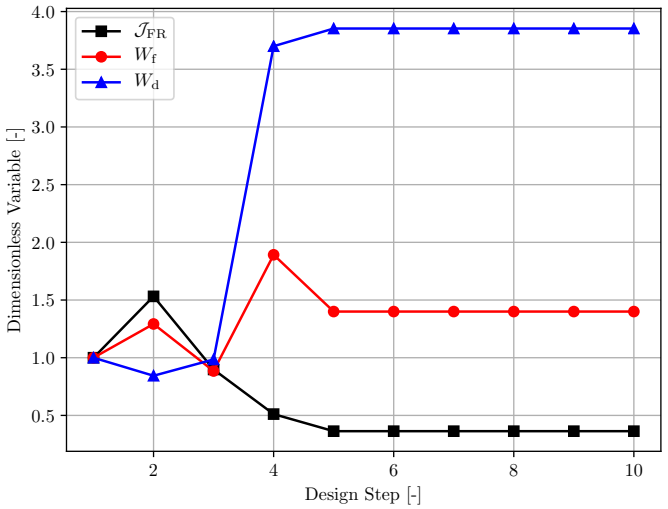

FIGURE 9: Optimization history of forced response minimization for the supersonic impulse turbine rotor.

the choice of a rather conservative value of A_f.

The mean pressure distribution of the optimized blade indicates that the majority of the shape changes are located in the mid part of the blade (see Figure 11, top). This can also be confirmed by looking at the baseline and optimized blade geometry plotted in Figure 12. The net result is the variation of the shock-wave pattern along the flow passage, which also influences the alternating pressure distribution.

Additionally, it can be noticed that the alternating pressure peaks shift upstream and increase in magnitude. This can be deemed contradictory at first. However, the work is also a function of the grid velocity, which becomes lower close to the axis of rotation. Consequently, a positive effect on the objective function can also be achieved at the expense of an increase of the unsteady loading.

Figure 13 illustrates the work distribution along both the baseline and the optimized blade. It can be seen that the forcing work in the optimized geometry slightly increases (see Figure 13, top). Nevertheless, such an increase is more than compensated by the significant increase of the negative damping-work within 0.5-0.8 of the chord-length, which has a net stabilizing effect on the blade vibrations, eventually making the impulsive airfoil less prone to aero-elastic failure.

CONCLUSIONS

The objective of this work was the development of a cost-effective adjoint-based forced response optimization framework. The developed framework implements an uncoupled aero-elastic analysis procedure based on the energy method, in conjunction with a multi-frequency harmonic-balance method for fully-turbulent quasi periodic unsteady flows.

The capability of the method was assessed by performing the numerical optimization of two exemplary turbomachinery blades, namely, that of a transonic compressor cascade and that of a supersonic impulse turbine rotor operating with toluene as working fluid. The following conclusions can be drawn from the outcomes of the study

1. The forced response is inherently dependent on both aero-forcing and aero-damping. Therefore, performing an optimization based only on one of the two phenomena does not guarantee the attainment of an optimized blade shape with superior aero-elastic performance.
2. Substantial improvements relate to forced response were obtained in relation to both the considered test cases. In particular, for the transonic compressor case, a 70% improvement in forced response was attained as a consequence of more than 50% reduction in aero-forcing and ∼2.5 times increase in aero-damping. For the supersonic impulse turbine, the optimization led to a reduction of the forced response by 60% as a result of a 1.5 times increase in aero-forcing and a 4 times increase in aero-damping.
3. In spite of the aeroelastic performance improvement, the entropy loss coefficient increased by 2 and 0.2 percentage points for the compressor and the turbine rotor test cases, respectively.
4. The computational cost of a single aero-elastic design iteration was in the order of 7 hours for the transonic compressor cascade test case (the cost of the adjoint solver being three times that of the flow solver) with ∼17 GB of memory consumption. Conversely, the cost for one design step for the

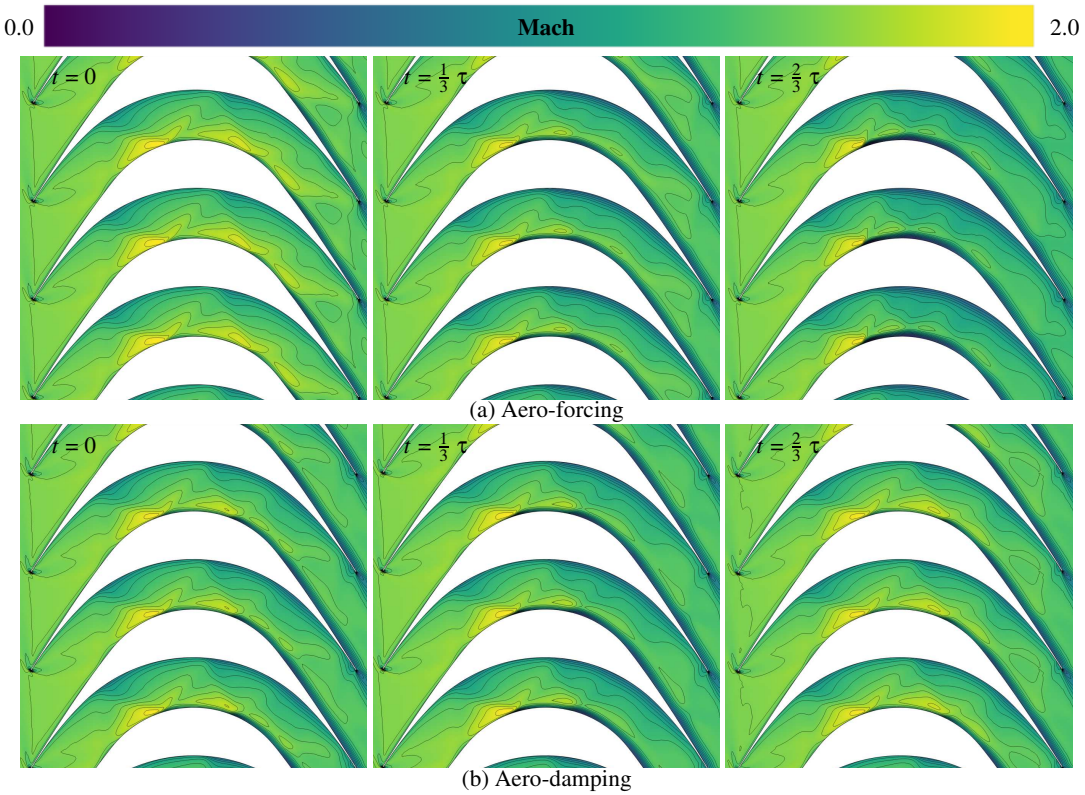

FIGURE 10: Mach number contours of the baseline geometry for supersonic impulse turbine rotor at three time slices, $t = 0$, $\tau/3$, $2\tau/3$, (a) Aero-forcing, (b) Aero-damping.

supersonic impulse turbine rotor case took approximately 6 hours, with ∼15 GB of corresponding memory requirement. A similar study performed using a gradient-based optimization based on finite-differences will take approximately 36 days per test case.

Future work will deal with the application of the proposed optimization framework to three dimensional problems, where the resonant frequencies, i.e., the frequencies at which forced response can occur, will be identified by means of a modal analysis method.

References

[1] Srinivasan, A. V., 1997. "Flutter and resonant vibration characteristics of engine blades: An igti scholar paper". *Journal of Engineering in Gas Turbines and Power,* **119**(4), June, pp. 742–775.

[2] Rinaldi, E., Pecnik, R., and Colonna, P., 2016. "Unsteady operation of a highly supersonic ORC turbine". *Journal of Turbomachinery,* **138**(12), June.

[3] Chahine, C., Vestraete, T., and He, L., 2019. "A comparative study of coupled and decoupled fan flutter prediction methods under variation of mass ratio and blade stiffness.". *Journal of Fluids and Structures,* **85**, pp. 110–125.

[4] Moffatt, S., and He, L., 2003. "Blade forced response prediction for industrial gas turbines part1: Methodologies". *Proceedings of ASME Turbo Expo 2003*.

[5] He, L., and Wang, D. X., 2011. "Concurrent blade aerodynamic-aero-elastic deisgn optimization using adjoint method". *Journal of Turbomachinery,* **133**(1).

[6] Engels-Putzka, A., Backhaus, J., and Frey, C., 2019. "Forced response sensitivity analysis using a adjoint harmonic balance solver". *Journal of Turbomachinery,* **141**(3), March.

[7] Mayorca, M. A., Vogt, D. M., Fransson, T. H., and Martensson, H., 2012. "A new reduced order modeling for stability and forced response analysis of aero-coupled blades considering various mode families". *Journal of Turbomachinery,* **5**(135), September.

[8] Carta, F. O., 1967. "Coupled blade-disk-shroud flutter instabilities i turbojet engine rotors". *Journal of Engineering for Gas Turbine and Power,* **89**(3), July, pp. 419–426.

[9] Ning, W., Moffatt, S., Li, Y., and Wells, R. G., 2003. "Blade forced response prediction and industrial gas turbines part 2: Verification and application". *Proceedings of ASME*

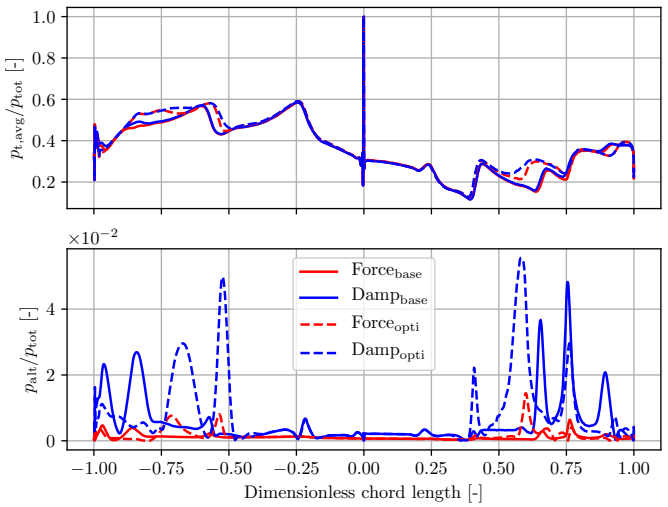

FIGURE 11: Time averaged (top) and alternating (bottom) surface pressure for the aero-forcing (red) and -damping (blue) calculation, for baseline (solid) and optimized (dashed) geometry. Positive and negative values of chord-length represent pressure and suction side.

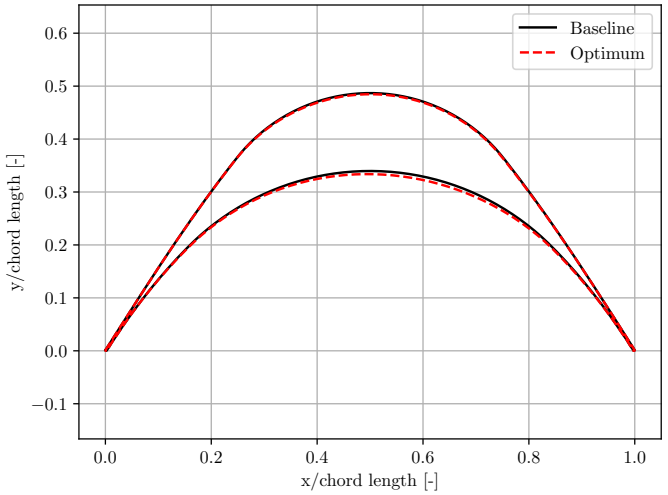

FIGURE 12: Baseline (solid) and optimized (dashed) geometry of supersonic impulse turbine rotor.

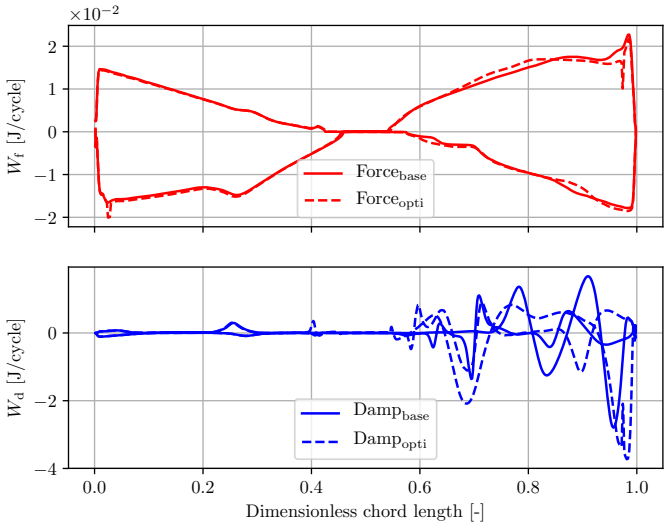

FIGURE 13: Local work plot for aero-forcing (top) and -damping (bottom) computation for baseline (solid) and optimized geometry (dashed).

Turbo Expo 2003(38642), June.

[10] Gopinath, A., van der Weide, E., Alonso, J., Jameson, A., Ekici, K., and Hall, K., 2012. "Three-dimensional unsteady multi-stage turbomachinery simulations using the harmonic balance technique". *45th AIAA Aerospace Sciences Meeting and Exhibit, Reno Nevada*.

[11] Yao, W., and Marques, S., 2018. "A harmonic balance method for nonlinear fluid structure interaction problems". *Computers & Structures,* **201**, May, pp. 26–36.

[12] Rubino, A., Pini, M., Colonna, P., Albring, T., Nimmagadda, S., Economon, T., and Alonso., J., 2018. "Adjoint-based fluid dynamic design optimization in quasi-periodic unsteady flow problems using a harmonic balance method.". *Journal of Computational Physics,* **372**.

[13] Vitale, S., Albring, T. A., Pini, M., Gauger, N. R., and Colonna, P., 2017. "Fully turbulent discrete adjoint solver for non-ideal compressible flow applications". *Journal of the Global Power and Propulsion Society,* **1**, pp. 252–270.

[14] Colonna, P., and Rebay, S., 2004. "Numerical simulation of dense gas flows on unstructured grids with an implicit high resolution upwind Euler solver". *International Journal for Numerical Methods in Fluids,* **46**(7), pp. 735–765.

[15] Anand, N., Vitale, S., Colonna, P., and Pini, M., 2018. "Assessment of FFD and CAD-based shape parametrization methods for adjoint-based turbomachinery shape optimization.". *Global Power and Propulsion Conference, Montreal.*, p. 8.

[16] Fransson, T. H., and Verdon, J. M., 1991. "Updated report on "standard configurations for unsteady flow through vibration axial-flow turbomahine-cascases". *Royal Institute of Technology*, July.

[17] Goldman, L. J., 1968. "Analytical investigation of supersonic turbomachinery blade, ii-analysis of impulse turbine-blade sections". *National Aeronautics and Space Administration*.

[18] Ghidoni, A., Pelizzari, E., Rebay, S., and Selmin, V., 2006. "3D anisotropic unstructured grid generation". *International Journal for Numerical Methods in Fluids,* **51**, pp. 1097–1115.

[19] Spalart, P. R., and Allmaras, S. R., 1992. "A one-equation turbulence model for aerodynamic flows". *AIAA Journal,* **1**, pp. 5–21.

[20] Kraft, D., 1988. "A software package for sequential quadratic programming". *Forschungsbericht-Deutsche Forschungs- and Versuchsanstaly fur Left- and Raumfahrt*.

[21] Virtanen, P., Gommers, R., Oliphant, T. E., Haberland, M., Reddy, T., Cournapeau, D., Burovski, E., Peterson, P., Weckesser, W., Bright, J., van der Walt, S. J., Brett, M., Wilson, J., Jarrod Millman, K., Mayorov, N., Nelson, A. R. J., Jones, E., Kern, R., Larson, E., Carey, C., Polat, İ., Feng, Y., Moore, E. W., Vand erPlas, J., Laxalde, D., Perktold, J., Cimrman, R., Henriksen, I., Quintero, E. A., Harris, C. R., Archibald, A. M., Ribeiro, A. H., Pedregosa, F., van Mulbregt, P., and Contributors, 2019. "SciPy 1.0–Fundamental Algorithms for Scientific Computing in Python". *arXiv e-prints*, Jul, p. arXiv:1907.10121.

[22] Paniagua, G., Iorio, M., Vinha, N., and Sousa, J., 2014. "Design and analysis of pioneering high supersonic axial turbines". *International Journal of Mechanical Sciences,* **89**, pp. 65 – 77.